American Journal of Applied Chemistry
2021; 9(6): 171-185
http://www.sciencepublishinggroup.com/j/ajac
doi: 10.11648/j.ajac.20210906.11
ISSN: 2330-8753 (Print); ISSN: 2330-8745 (Online)

Formulation and Characterization of Light Aggregates from Phosphate Ore Processing Waste from the Hahotoe and Kpogame Mines, Potential Use for Agricultural Applications

Moursalou Koriko[1, *], Dodji Zounon[1], Diyadola Diheenane Bafai[1], Sanonka Tchegueni[1], Koffi Agbegnigan Degbe[1], Koffi Fiaty[2], Patrick Drogui[3], Gado Tchangbedji[1]

[1]Waste Management Treatment and Recovery Laboratory (GTVD), Lome University, Lome, Togo

[2]Automatic Control Chemical and Pharmaceutical Engineering Laboratory (LAGEPP), Claude Bernard Lyon-1 University, Lyon, France

[3]Water Earth Environment Center, The National Institute for Scientific Research (INRS), Quebec, Canada

Email address:

mkoriko@univ-lome.tg (M. Koriko)

[*]Corresponding author

To cite this article:

Moursalou Koriko, Dodji Zounon, Diyadola Diheenane Bafai, Sanonka Tchegueni, Koffi Agbegnigan Degbe, Koffi Fiaty, Patrick Drogui, Gado Tchangbedji. Formulation and Characterization of Light Aggregates from Phosphate Ore Processing Waste from the Hahotoe and Kpogame Mines, Potential Use for Agricultural Applications. *American Journal of Applied Chemistry.* Vol. 9, No. 6, 2021, pp. 171-185. doi: 10.11648/j.ajac.20210906.11

Received: October 14, 2021; **Accepted**: November 4, 2021; **Published**: November 10, 2021

Abstract: This study relates to the development of light aggregates from phosphate sludge, rejects to sieves and clays. Three types of aggregates denoted S9, S10 and S11 have been developed. Samples S9 are composed of clay, screenings and phosphate sludge, samples S10 of clay and screenings and samples S11 of clay and phosphate sludge. The influence of temperature and cooking time on the properties (water absorption, density, porosity, etc.) of the aggregates produced was studied, as well as their mineralogical composition. For this purpose, three different cooking temperatures 900°C, 950°C and 1000°C, and two cooking times 30 and 60 min were considered. This study showed that the water absorption of aggregates cooked for 30 min varies between 12.71% and 14.93% while that of aggregates cooked for 60 min varies between 12.78% and 15.16%. The lowest water absorption is observed at the S10 aggregates sintered at 900°C for 30 min while the highest water absorption is observed at the S9 aggregates sintered at 900°C for 60 min. The dry density of aggregates cooked for 30 min varies between 1.27 and 1.68 g/cm^3 while that of aggregates cooked for 60 min varies between 1.75 and 2.13 g/cm^3. With the exception of S11 aggregates baked at 950 and 1000°C for 60 min, which have their density greater than 2 g/cm^3, all the others can be considered light aggregates. It should also be noted that the aggregates cooked for 30 min have a lower density than the aggregates cooked for 60 min. The porosity of the aggregates cooked for 30 min varies between 16.30 and 20%, on the other hand the aggregates cooked for 60 min varies between 19.06 and 23.64%. X-ray diffraction analysis of the aggregates shows that they are mainly composed of fluoroapatite, quartz, hematite and plagioclases (albite, labradorite, and anorthite). The study also showed that the amount of quartz and fluoroapatite decrease with temperature. On the basis of the physical and mineralogical analysis carried out on the light aggregates, we could find them suitable for agricultural applications, especially their uses as substrates in hydroponics, in greenhouse cultivation in general, and in gardening.

Keywords: Phosphate Sludge, Screen Refusal, Clays of Aklakou, Formulation, Characterization, Light Aggregates, Applications, Amendments, Agriculture

1. Introduction

One of today's major economic and environmental problems is the generation and treatment of large volumes of waste produced continuously by industries. Among these waste-producing industries, we cite the mining industry

criticized for the management of mining waste produced during the exploitation of mineral deposits.

Thanks to their generous subsoil, African countries have an economy that is essentially based on the exploitation of mineral resources. But the waste generated by the exploitation of mining resources is a great source of pollution, and represents real ecological scourges that threaten this big continent. This threat already hangs on Togo, a country in West Africa. The exploitation of phosphate in the Togolese subsoil, which began in 1957 [1], has resulted in the pollution of terrestrial and marine ecosystems [2].

This pollution is manifested on the one hand by the emission of dust and gaseous waste that contaminate the air we breathe, and on the other hand by the discharge of sludge and liquid waste into the sea. While the air pollution is localized for the moment, the waste discharged into the ocean spreads along the Atlantic coast under the effect of marine currents. This pollution can be seen in the coloring of the ocean for up to 400 meters of the coast [3].

The pollution of the sea on the coast has caused the removal or even the death of fish, and consequently the decline of fishing activities. In addition, according to recent studies, the consumption of hyper-phosphate fish would lead to an increase in bone leakage, which in turn leads to a reduction in bone density. In Togo, an average of 2.5 million tons of phosphate waste are discharged into the sea each year despite the health and ecological consequences [4-6].

This situation increasingly encourages the development of alternative and economically viable and options for reuse and recycling.

Industrial waste cannot be considered only as a waste but rather as a by-product or deposits of one or more elements of commercial value. The current waste management methods are inadequate and lead to negative impacts on the environment and an excessive consumption of non-renewable natural resources (clays, sand, etc...). Indeed, the reuse of mining wastes can be done outside the mining site, depending on their physicochemical and mineralogical composition. Thus, the field of construction can constitute an attractive channel to absorb industrial and mining mineral by-products [7]. This alternative is nowadays a very promising environmental solution, and has become very popular in terms of reducing the exhaustive use of non-renewable natural resources in the field of construction materials, and reducing the costs of storage and maintenance of industrial and mining wastes stored in tailings facilities. Several recovery methods with more or less complex pre-treatment of solid waste have been evaluated. To mention only the most important ones: concrete, mortar, roads, ceramics and cement.

Among others, thermal treatment techniques are currently considered as a promising alternative for the treatment and/or recovery of mining waste.

This pathway allows a significant reduction in the waste volumes, physical and chemical stabilization of toxic pollutants and/or recovery of waste into useful materials such as clay bricks and light aggregates [8-10, 44] or light weight ceramic products with good acoustic and thermal insulation [45].

Among these thermal treatment methods, we have chosen to recover phosphate waste into light aggregates. Indeed, the light aggregates have many applications, among which we can mention: the production of light concretes, geotechnical backfill, insulation products, soils, hydro-culture, drainage, roof-gardens, recycling of hazardous waste and filters [11-14].

Recently Amrani and col [43] investigate an approach of phosphate valorization in producing asphalt mixtures which according to the authors can be a cost-effective and eco-friendly solution for managing the wastes. Furthermore, El Machi and al [46] discuss the use of stone-removal waste-rocks from phosphate mine as aggregates for concrete formulation as a full replacement of natural aggragates in order to improve their mechanical behavior performance according to the required standards.

With a density less than 2 g/cm^3, light aggregates typically weigh less than three-quarters of normal weight aggregates. As a result, the use of light aggregates can reduce the demand for reinforced steel and cement, thereby reducing construction costs. In addition, light aggregates can reduce the rate of heat conduction due to their abundant pores, which helps air conditioner users to save energy in hot weather.

This study aims to carry out a detailed analysis of the constituent components of phosphate wastes to propose a better method for synthesizing light aggregates. Determining of the physical properties of light aggregates such as density, compressive strength, water absorption, porosity are an important step to achieve this goal [15-17].

Previous studies conducted by Koriko et al [41] indicated that Aklakou's clay with a high aluminosilicate content can be used to amend the tailings from the phosphate mines of Hahotoe and Kpogame in Togo [42] in order to valorize them into light aggregates that can be potentially used in agriculture and construction.

2. Materials and Methods

2.1. Sampling

A one-week sampling campaign was carried out in order to collect the waste: phosphate sludge (Figures 1(a)) and screen refusals (Figure 1(c)) resulting from the treatment of the natural phosphate at the Kpémé phosphate processing site. Clay sampled (Figure 1(b)) from the Aklakou site was used to amend the waste [41]. After collection, the phosphate sludge was decanted, dried, crushed and then sieved to obtain powders with a particle size less than or equal to 150 µm. Apart from decantation, screen refusals and clay underwent the same preparation steps as described above.

(a) Phosphate washing sludge (b) Clay of Aklakou (c) Waste from rejection to screens

Figure 1. *Different samples used.*

2.2. Manufacture of Aggregates

The aggregates elaboration method consists of three steps: preparation of raw materials, preparation of raw aggregates and finally sintering or firing step [18]. In the first step the raw materials are dried, crushed and sieved into fractions of fairly similar sizes [19, 20]. The preparation of the raw aggregates is carried out from the following mixtures:

Mixture denoted S9: 60% of clay + 30% of screen refusal + 10% of phosphate sludge;

Mixture denoted S10: 60% of clay + 40% of screen refusal;

Mixture denoted S11: 60% of clay + 40% of phosphate sludge.

To prepare the paste, the mixtures are moistened with distilled water up to 30% by weight according to the protocol described by Loutou et al [21], then the paste is shaped in the form of pellets with diameters of about 8 to 12 mm. The pellets are then dried at room temperature for 48h, then oven dried at a temperature of 105°C ± 10°C for 72h and finally sintered or fired for 30 min or 60 min at three different temperatures of 900°, 950° and 1000°C, at a speed of 10°C/min in an electric oven. The obtained aggregates are naturally cooled down to room temperature in the switched off furnace.

2.3. Characterization of Materials

The physicochemical characterization of the raw materials was carried out in laboratories in France and Canada. The main characterization methods used are the following:

Atomic Emission Spectroscopy

Inductively Coupled Plasma Atomic Emission Spectrometry (ICP-AES) was used in this study to determine the chemical composition of the study materials [22]. The elemental analysis of solid phases by ICP-AES requires a mineralization step of the sample to completely solubilize it. Mineralization was done by alkaline fusion or digestion with aqua regia [23]. The spectrometer used in this study is ICP-AES Dual View 5110. The chemical analysis was carried out at Water Earth Environment Center of the National Institute for Scientific Research (INRS) of the University of Quebec Trois Rivières (UQTR).

Differential thermal analysis and thermogravimetry

The thermal behavior was performed using thermogravimetric analysis (TGA) a technique that consists of measuring the loss of mass of a sample as a function of time, for a given temperature or temperature profile [24]. To perform these analyses, a mass between 18 g and 40 g of the sample to be analyzed is placed in an alumina crucible and the control sample in another crucible of the same nature. The apparatus used is of the type "NETZSCH TG 209F122-10-210-K" equipped with an oven allowing to reach temperatures up to 1200°C. Analyses were performed in a temperature range from room temperature about 25°C to 1000°C under a nitrogen gas stream. The temperature gradient was set at 10°C/min. Thermogravimetric (TGA) and Differential Thermal (DTA) analysis of samples were performed in the Laboratory of Automatic Control, Chemical Engineering and Pharmaceutical processing (LAGEPP) of University Claude Bernard Lyon-1 (France).

X-ray diffraction analysis

X-ray Diffraction (XRD) allows the determination of the mineral phases of these materials. To perform this analysis, a monochromatic and parallel X-ray beam strikes a crystal and is diffracted in a given direction by each of the families of reticular planes each time the condition or Bragg's law is realized [25, 26]. The analysis were performed in the LAGEPP laboratory using a Seifert XRD 3000 TT diffractometer with experimental details of data collection summarized in Table 1. The processing of the results was performed using the software "QualX". The indexation of the phases is based on the comparison of the real diffractograms with the diffractograms of the POW_COD files database by comparison of the inter-reticular distances.

Table 1. *Experimental details of X-ray powder-profile data collection.*

Radiation	Cu, $K\alpha_{1,2}$, $I(\lambda_1)/I(\lambda_2) = 0.5$
Divergence slits	3.00 mm –Soller–2.00 mm
Receiving slits	–Soller–0.10 mm
2θ Range (°)	8 – 160
Step scan	θ – θ
Step width (2θ)	0.02°
Counting time (s) [range (°2θ)]	30 [8-60], 40 [60-100], 50 [100-160]
Sample	Powder (particle size<90 µm) compressed in cylindrical sample holder of 24 mm diameter and 0.5 depth
Temperature	Room temperature (293 K)

Analysis by Fourier Transform Infrared Spectroscopy

Fourier Transform Infrared Spectroscopy (FTIR) is based on the absorption of infrared radiation by the analyzed material. It allows the detection of vibrations characteristic of chemical bonds, to perform the analysis of functional groups present in materials [27, 28]. The FTIR analysis was performed on KBr pellets containing homogeneous mixture of 2 mg of compound and 300 mg KBr in the LAGEPP laboratory. The device used is the VERTEX70 type. IR scan was performed from 400 to 4000 cm^{-1}.

Scanning electron microscopy analysis coupled with X-ray Dispersive Energy microanalysis (SEM-EDX).

The device used "XL30 PHILIPSESEM" is equipped with an EDX probe. The acceleration voltage is 30 kV and the lateral resolution is 2.5 nm. Samples analysis were performed at LAGEPP Laboratory (France).

2.4. Characterization of Light Aggregates

For the characterization of the aggregates, two physical properties were determined, namely density and water absorption.

Water absorption

Water absorption is determined by weighing the masses of the aggregates before (m_{av}) and after immersion (m_{ap}) in water for 24 h. Then the water absorption is calculated according to relation (1):

$$AE = \frac{m_{ap}-m_{av}}{m_{av}} x100 \quad (1)$$

Dry density and porosity of light aggregates

Let us denote by M_0 the mass of the dry sample before immersion in water, M_1 the mass of the aggregates saturated with water on the surface, M_2 the mass in the pycnometer containing aggregates and water and by M_3 the mass of the pycnometer containing water. The dry density is the ratio of the mass of a sample of dried aggregates to the volume of these aggregates in water, including the volume of pores to which water is accessible and the sealed internal pores [29]. It was also measured by pycnometry using distilled water as solvent. It's expressed by:

$$d = \frac{M_0}{M_1-(M_2-M_3)} \quad (2)$$

All the tests were repeated three times and the calculated average values are used for density and porosity estimation. Porosity is then determined from the following relationship (3):

$$Po = 100x \frac{M_1-M_0}{M_0-(M_2-M_3)} \quad (3)$$

3. Results and Discussion

Elaboration of aggregates

The different aggregates S9, S10 and S11 produced at different temperatures are shown in Figure 2. They have largely retained their original, mainly spherical shape. The S9 and S10 aggregates have a homogeneous red-brown color over their entire surface. Pores or cracks on the surface of these pellets are rarely visible. On the other hand, aggregates S11 have mostly pores and cracks reaching the surface of the pellets. Their color is grey to grey-black. Table 2 shows the content of oxides in the different aggregates and their ratio to the melting components (Na_2O, K_2O, CaO, MgO and Fe_2O_3) . On Figure 3 is represented the composition diagram of Riley for the aggregates. The analysis of Table 1 and the Riley composition diagram shows that the chemical compositions of the mixtures respect one of the conditions for having light aggregates. Indeed the locations of the three mixtures are in the swelling zone on the Riley composition diagram. They have an abundance of melting components. Since the gas-producing constituents are in most cases the melting elements, then there will be a gas input during firing. If $\frac{\%SiO_2}{\sum F} \geq 2$ with $\sum F = \%Na_2O + \%K_2O + \%CaO + \%MgO + \%Fe_2O_3$, the total quantity of melting elements then we will have a sufficient amount of liquid phase to make the materials transform into a viscous state. On the other hand if $\frac{\%SiO_2}{\%Al_2O_3} \geq 4$ then we can have a liquid phase viscosity suitable for trapping and growth of gas bubbles that leads to bloating [30].

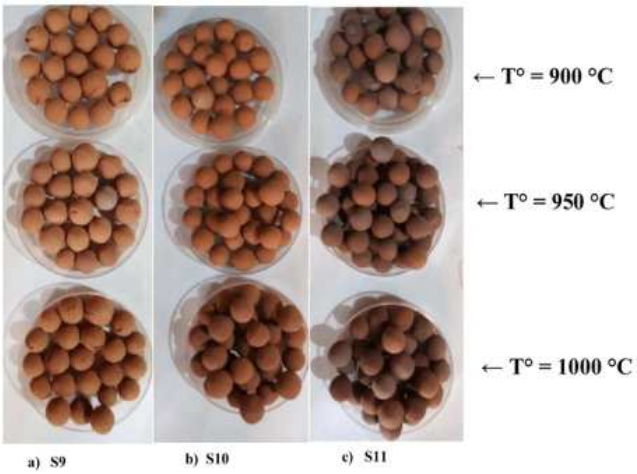

Figure 2. *Different aggregates developed.*

Table 2. *Ratio of oxides in the aggregates.*

Aggregates	% SiO_2	% Al_2O_3	∑F	%SiO_2/∑F	%SiO_2/%Al_2O_3
S9	54.572	13.969	23.286	2.34	3.91
S10	54.48	8.28	31.05	1.75	6.58
S11	54.85	9.16	17.88	3.07	5.99

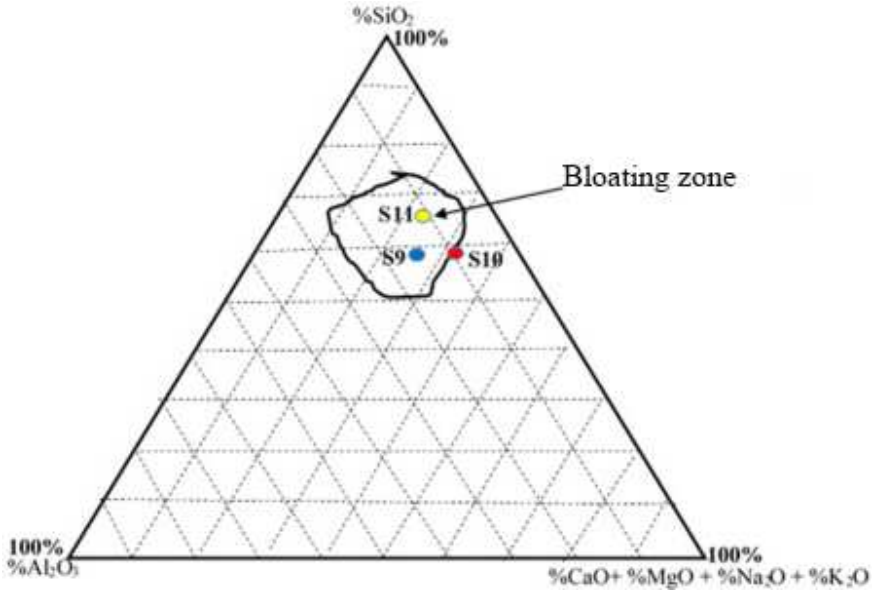

Figure 3. *Riley's composition diagram for the mixtures.*

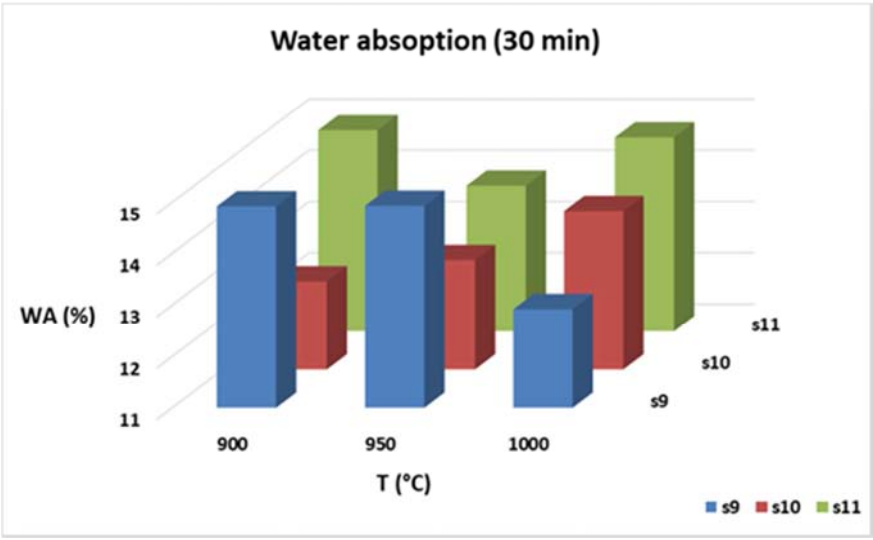

Figure 4. *Diagram of the variation in water absorption of sintered aggregates for 30 min.*

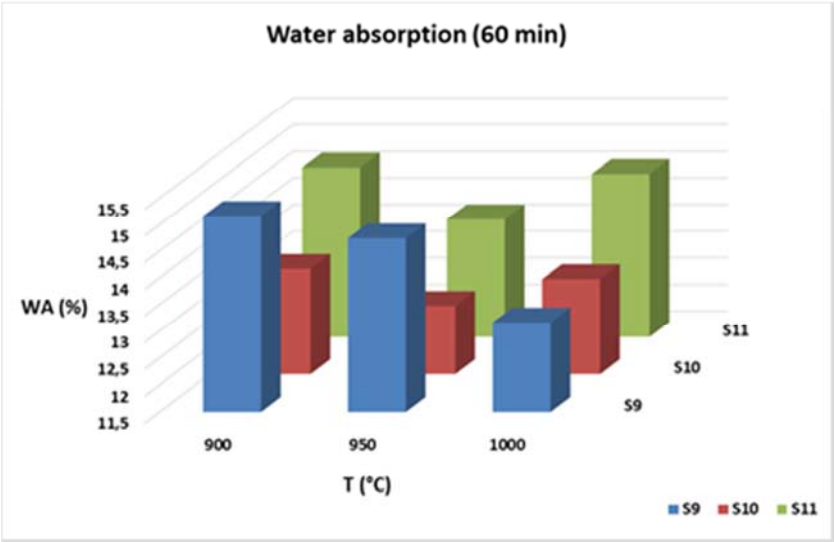

Figure 5. *Diagram of the variation in water absorption of sintered aggregates for 60 min.*

Water absorption results of the different series of aggregates are plotted in Figures 4 and 5. Water absorption of the aggregates fired for 30 min varies between 12.71% and 14.93% while that of the aggregates fired for 60 min varies between 12.78% and 15.16%. The lowest water uptake is observed in the S10 aggregates sintered at 900 ° C for 30 min while the highest water uptake is observed in the S9 aggregates sintered at 900°C for 60 min. We notice that the water uptake of the aggregates sintered for 60 min decreases with temperature. This could be explained by the densification of the structure, the decrease of the porosity under the effect of the temperature increase. The size and amount of pores formed are also determinants of variations in water uptake of the aggregates. If the pores formed are not interconnected this could also explain the decrease in water absorption [31]. For an aggregate with isolated pores or a vitrified surface tends to absorb little water, whereas a particle with connected or open pores will adsorb water like a sponge [31]. This will be confirmed by the results of SEM analysis.

Dry densities of the manufactured aggregates baked for 30 min are plotted in the diagrams in Figure 6 while those of the aggregates baked for 60 min are plotted in Figure 7. The dry density of the aggregates baked for 30 min varies between 1.27 and 1.68 g/cm^3. All the aggregates baked for 30 min have their density lower than 2 g/cm^3, they could be considered as light aggregates. On the other hand, the dry densities of the aggregates baked for 60 min varied between 1.75 and 2.13 g/cm^3. The analysis of the results shows that the densities of the aggregates cooked for 60 min increase with temperature. We can then deduce that the aggregates tend to contract with increasing temperature and baking time. Note that the S11 aggregates fired at 950 and 1000 °C for 60 min do not meet the criteria to be considered as light aggregates due to the fact that their densities exceed 2 g/cm^3. On the other hand, the other S9 aggregates fired for 60 min have relatively low densities (< 2 g/cm^3) and can, therefore, be considered as light aggregates [32].

We find that the densities of the aggregates baked for 30 min are lower than the densities of the aggregates baked for 60 min while the water uptake of the aggregates baked for 60 min is higher than those baked at 30 min. This may be due to the fact that the pores formed at the 30 min baked aggregates are not interconnected [33].

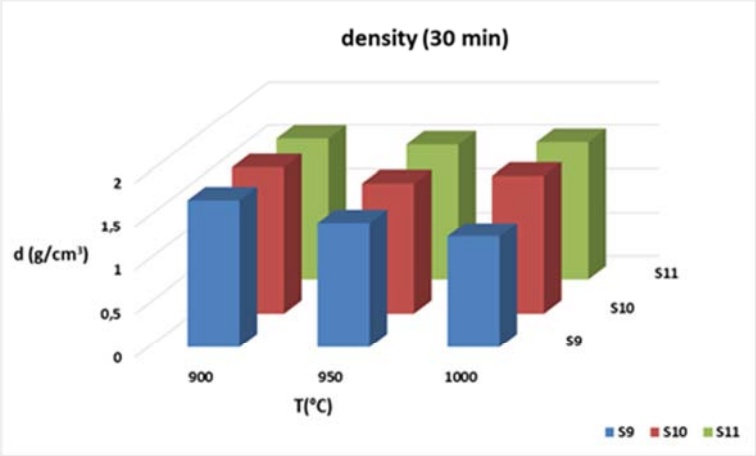

Figure 6. *Diagrams of the change in dry density of sintered aggregates for 30 min.*

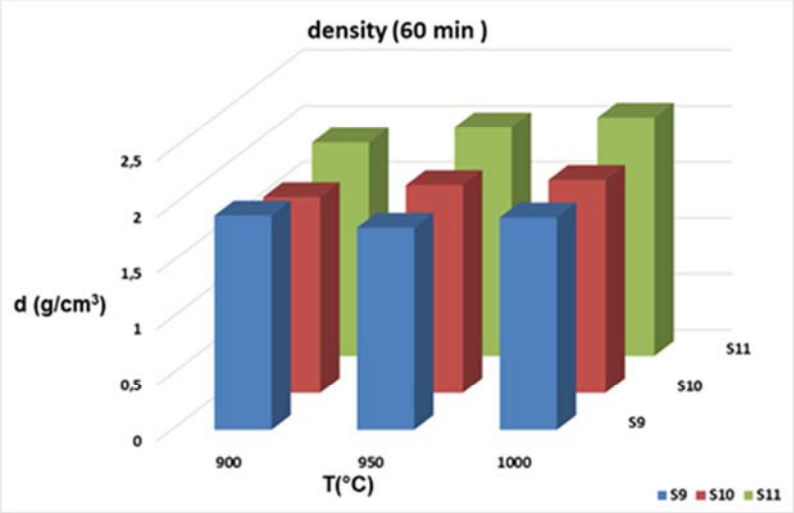

Figure 7. *Diagrams of the change in dry density of sintered aggregates for 60 min.*

On Figures 8 and 9 are depicted the evolutions of the porosity of the aggregates baked during 30 min and 60 min respectively. The observed trends of these curves show a variation of the porosity of the aggregates baked during 30 min between 16.30 and 20% (Figure 8), whereas that of the aggregates fired during 60 min vary between 19.06 and 23.64% (Figure 9).

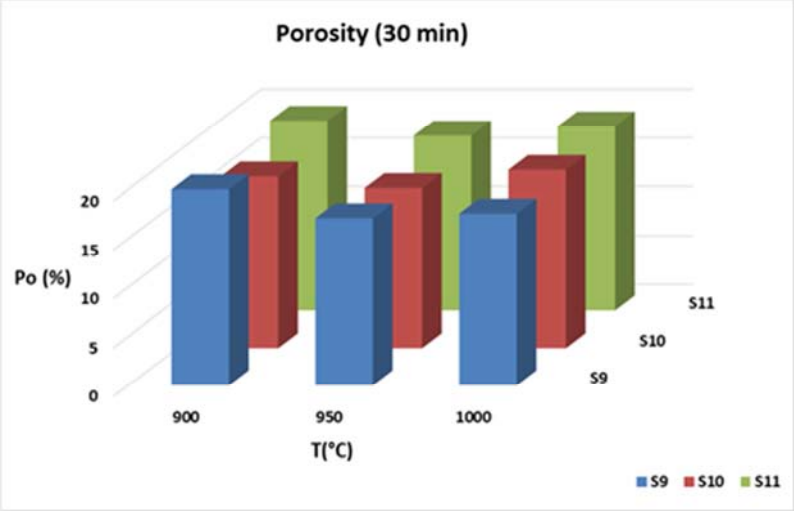

Figure 8. *Diagram of the variation in porosity of sintered aggregates for 30 min.*

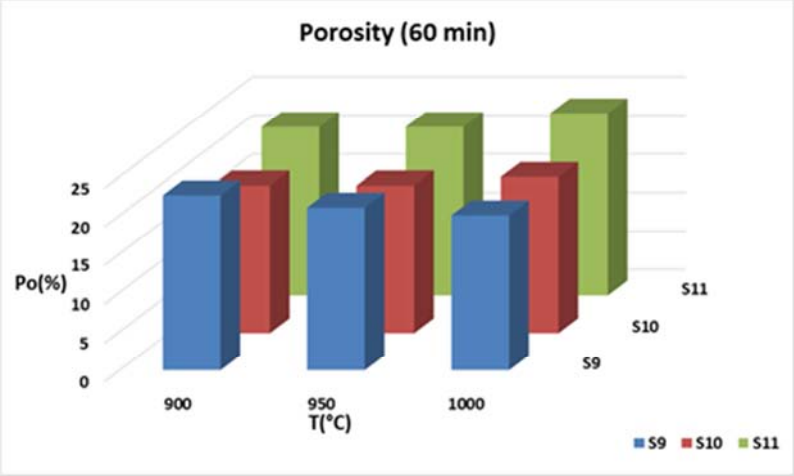

Figure 9. *Diagram of the variation in porosity of sintered aggregates for 60 min.*

The porosity of aggregates baked for 60 min remains higher than that of aggregates baked for 30 min. Thus, it appears that aggregates fired for 60 min have more pores accessible to water than aggregates fired for 30 min [17]. The sintering time of 30 min may result in an incomplete reaction leading to insufficient gas evolution to form pores in the pellets. This could also be explained by the fact that the pores formed at the aggregates fired for 30 min are not all interconnected.

Mineralogical and morphological characterization of light aggregates baked for 60 min

X-ray diffractograms of S9 aggregates fired at temperatures of 900°C, 950°C and 1000°C are shown in Figure 10. Analysis of these diffractograms shows that they are mainly composed of fluoroapatite, quartz and hydroxyapatite. From the initial composition of the mixture, we can deduce the disappearance of kaolinite in the aggregates. Indeed, the dehydroxylation of kaolinite takes place at a temperature lower than 600°C [34]. This last result is corroborated by the thermal analysis carried out on the raw materials. Moreover, Santos et al [35] have shown that above 500°C, kaolinite ($Si_2Al_2O_5(OH)_4$) is transformed into metakaolin ($Si_2Al_2O_7$) but the reflections of the metakaolin were diffuse and weak so its peaks do not appear on the diffractograms of S9 aggregates.

On the other hand, quartz is still present in the aggregates, however its quantity decreased with temperature. This is due to the transformation of quartz into amorphous silica with increasing temperature [36, 37].

The structural characterization of the phosphate rejects used in the elaboration of the aggregates revealed that they are constituted mainly of carbonated fluoroapatite [38] which is not the case of the fluoroapatites detected in the aggregates. This result can be explained by the decomposition of the carbonate in the range of 700 to 900°C

[34]. It should also be noted that at higher temperatures partial substitution of calcium or fluorine was observed in fluoroapatites (Figure 10c). Hydroxyapatite detected in the aggregates could come from the partial transformation of the fluoroapatite. Analysis of its diffractograms also reveals that the amount of hydroxyapatite increases with temperature.

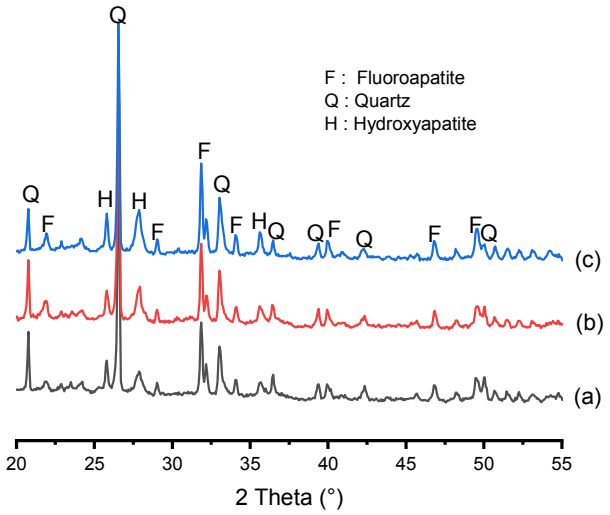

Figure 10. *X-ray diffractograms of S9 aggregates baked for 60 min at 900°C (a), 950°C (b) and 1000°C (c).*

We can therefore deduce that the increase in temperature favors the substitution of fluoride ions (F^-) in the fluoroapatite by hydroxide ions (OH^-).

Concerning the effect of the 60 min firing time on the nature of the aggregates obtained, density analysis revealed that only the S9 aggregates fired for 60 min presented relatively low densities (< 2 g/cm^3) and could be considered as light aggregates. For this reason we were interested in the electron microscopic (SEM) and energy dispersive spectrum (EDX) characterization of the S9 samples developed at temperatures of 900°C, 950°C and 1000°C. The results obtained are shown in Figure 11 for SEM and those of EDX in Figure 12.

Scanning microscopy allows to observe the texture of samples and to characterize mineralogical assemblages. The clay particles appear as clusters of fine aggregates and rod-shaped platelets with irregular contours. This is a morphology found as well for poorly crystallized kaolinites as for illites as observed by Konan [39].

In parallel to the SEM images, we performed semi-quantitative EDX analysis of the samples for the determination of the chemical composition of the analyzed aggregates. All these Figures show the presence of chemical elements contained in the compounds (C, O, F, Na, Mo, Al, Si, K, Cl and Ca) (Table 3). It should be noted that a strong presence of silicon is due mainly to the most important content of quartz in the samples studied. These results confirm well those obtained through X-ray powder diffraction analysis which revealed the presence of quartz, fluoroapatite and hydroxyapatite (Figure 10), hence the high percentages of the element oxygen.

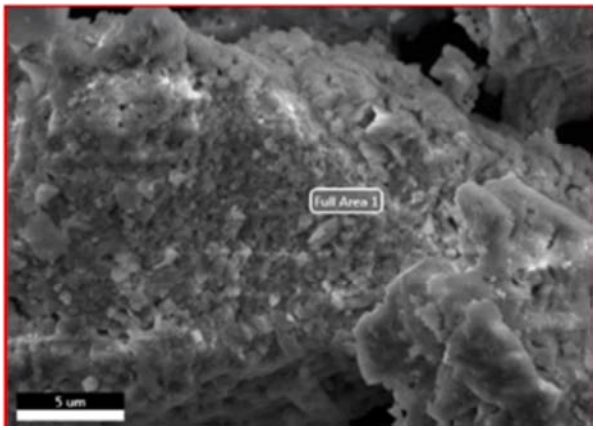

a) Specimen S9 fired at 900°C

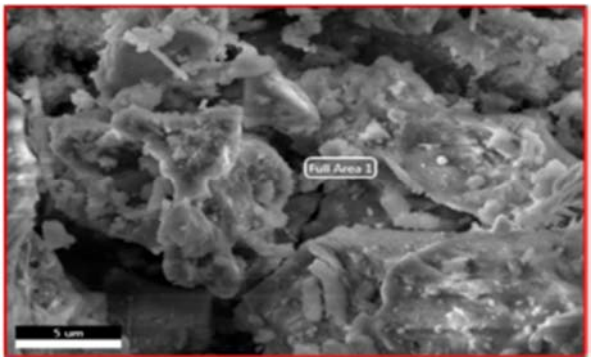

b) Specimen S9 fired at 950°C

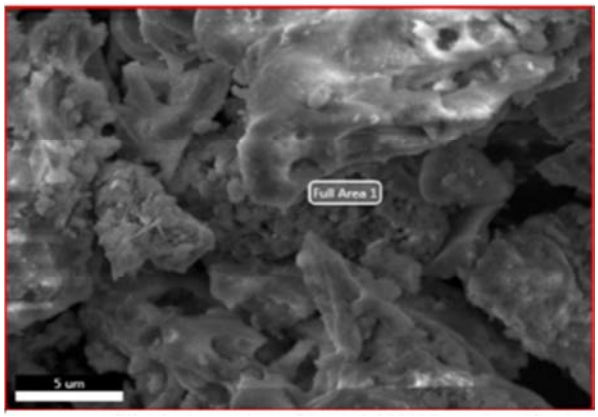

c) Specimen S9 fired at 1000°C

Figure 11. *SEM images of S9 aggregates baked for 60 min.*

Table 3. *Microanalysis of different chemical elements constituting the S9 aggregates at 900°C (a), at 950°C (b) and at 1000°C (c).*

a) Specimen S9 fired at 900°C

Element	% Mass	% Atomic
C K	0.35	0.69
O K	37.88	55.35
F K	2.25	2.77
NaK	0.11	0.11
MgK	0.53	0.51
AlK	6.62	5.73
SiK	10.38	8.64
P K	10.28	7.75
ClK	0.16	0.10
CaK	31.44	18.34

b) Specimen S9 fired at 950°C

Element	% Mass	% Atomic
O K	43.97	59.54
F K	0.25	0.28
FeL	3.10	1.20
NaK	0.16	0.15
MgK	1.07	0.95
AlK	15.54	12.48
SiK	24.72	19.06
P K	1.66	1.16
ClK	0.10	0.06
K K	0.73	0.40
CaK	8.71	4.71

c) Specimen S9 fired at 1000°C

Element	% Mass	% Atomic
O	42.57	59.33
F K	0.42	0.49
FeL	4.29	1.71
NaK	0.55	0.53
MgK	0.75	0.69
AlK	11.55	9.54
SiK	20.56	16.32
P K	3.82	2.75
ClK	0.11	0.07
K K	0.70	0.40
CaK	14.68	8.16

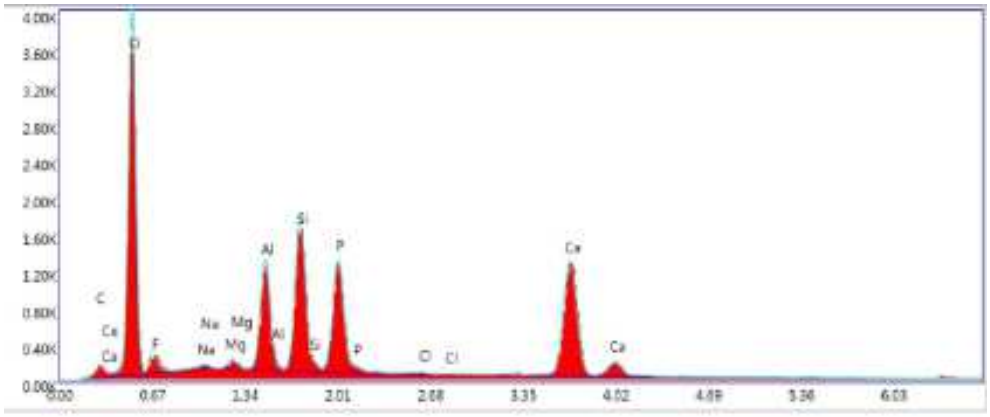

a) Specimen S9 fired at 900°C

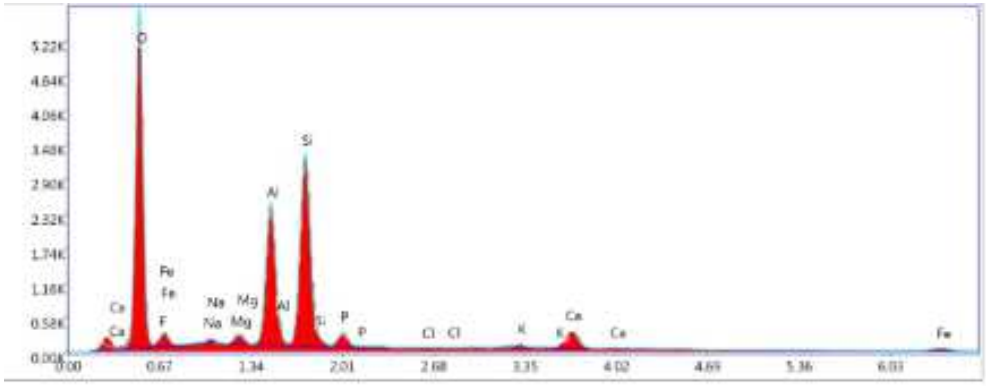

b) Specimen S9 fired at 950°C

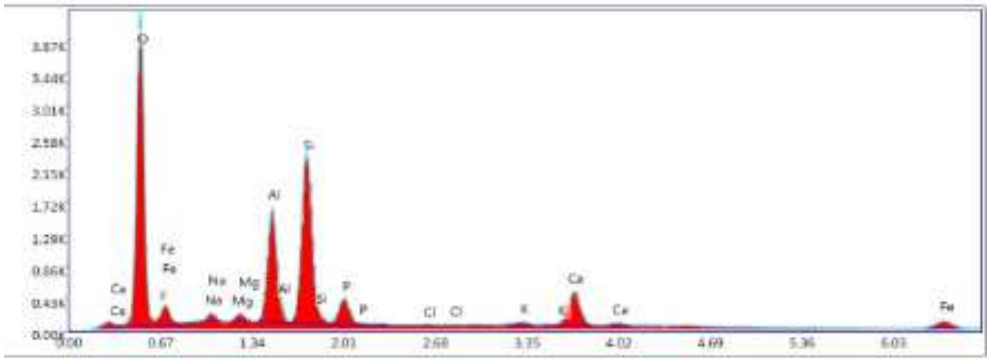

c) Specimen S9 fired at 1000°C

Figure 12. *Energy Dispersion Spectrum (EDX) and elemental analysis of S9 aggregates at 900°C, 950°C and 1000°C.*

Regarding the S10 light aggregates, the X-ray diffractograms for this aggregates fired at temperatures of 900°C, 950°C and 1000°C are shown in Figure 13. Analysis of these diffractograms also shows that they are mainly composed of fluoroapatite, quartz, hydroxyapatite and a secondary phases namely sodium calcium aluminosilicate ($Na_{0.48}Ca_{0.52}Al_{1.52}Si_{2.48}O_8$) as well as dipotassium cobalt (II) bis(dihydrogen phosphate) dihydrate ($K_2Co(H_2P_2O_7)_2, 2H_2O$). As in the S9 aggregates, we observe the disappearance of kaolinite in the S10 aggregates. This result is confirmed by the thermal analysiss performed on the raw materials. Quartz is still present in the S10 aggregates but its quantity decreased with temperature (Figure 13) as in the case of the S9 aggregates. This is also due to the transformation of quartz into amorphous silica when increasing temperature [36, 37]. The above result are in agreement with those found by Loutou et al [40].

Hydroxyapatite detected in S10 aggregates could result from the partial transformation of fluoroapatite. We also observe on the diffractograms that the amount of hydroxyapatite increases with temperature as previously observe on the X-ray diffractograms of S9 aggregates. Sodium calcium aluminosilicate (Figure 13c) is a mineral that belongs to the anorthite family. With regard to the chemical composition, namely CaO, SiO_2 and Al_2O_3 of the mixed materials, the presence of this phase in the aggregates is then predictable. Nevertheless we observe that it is absent in the diffractograms of the aggregates fired at 900°C and 950°C. This is due to the fact that this phase can only be formed at temperatures greater than or equal to 1000°C.

The dipotassium (II) bis (dihydrogen phosphate) dihydrate cobalt phase detected on the diffractogram of the S10 aggregates baked at 1000°C could result from the reaction between cobalt and fluoroapatite.

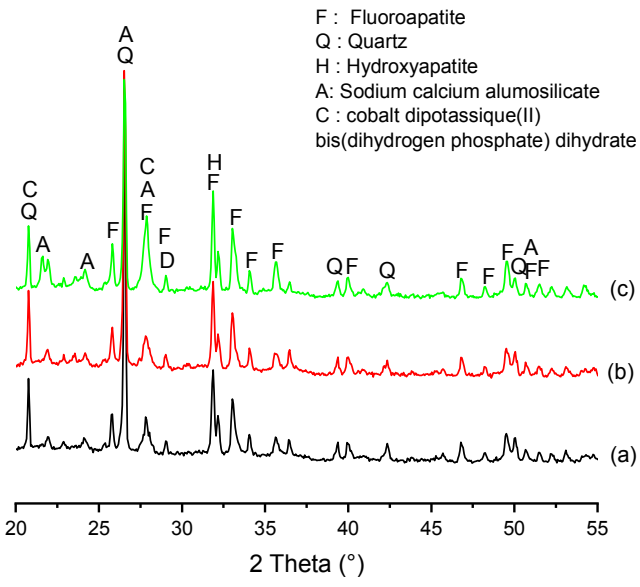

Figure 13. *X-ray diffractograms of S10 aggregates fired at 900°C (a), 950°C (b) and 1000°C (c).*

Finally, Figure 14 shows the X-ray diffractograms of the S11 aggregates baked at temperatures of 900°C, 950°C and 1000°C. These diffractograms also reveal the presence of fluoroapatite, quartz and hydroxyapatite phases. However we also note the presence of other major phases such as albite ($NaAlSi_3O_8$) and labradorite ($Al_{1.66}Ca_{0.66}Na_{0.34}O_8Si_{2.34}$). The minor phases present in the diffractograms are hematite (Fe_2O_3) and copper calcium divanadate ($CaCu(V_2O_7)$).

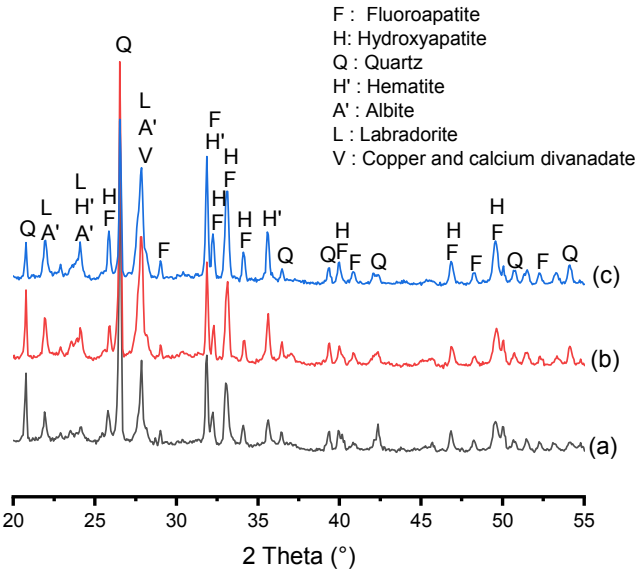

Figure 14. *X-ray diffractograms of S11 aggregates fired at 900°C (a), 950°C (b) and 1000°C (c).*

In these diffractograms it can be noticed always that the quantities of quartz decrease with the temperature. This only confirms the observations made previously on the aggregates S9 and S10, which is the conversion of the quartz into amorphous silica as the temperature increases [36].

The presence of fluoroapatite on the diffractograms shows that this phase is resistant to high temperatures (T°C < 1000°C). Nevertheless, the appearance of hydroxyapatite ($Ca_{10}(PO_4)_6(OH)_2$) among the phases in the aggregates indicates that some F^- ions in the fluoroapatite ($Ca_{10}(PO_4)_6F_2$) were substituted by the OH^- ions. We also observe that some calcium atoms of some hydroxyapatite phases revealed in the diffractograms were substituted by the cobalt atoms, as an example the $Ca_{8.85}Co_{1.15}(PO_4)_6(OH)_2$ phase identified on the diffractogram of the S11 aggregates fired at 950°C (Figure 14b).

The albite and labradorite phases belong to the plagioclase family of general formula $Na_xCa_{1-x}Al_{2-x}Si_{2+x}O_8$. The presence of these phases in the diffractograms is in agreement with the chemical composition of the mixed materials. Indeed, the phosphate slurries and the clay contain CaO, SiO_2 and Al_2O_3 which enter in the formation of plagioclases after a thermal transformation.

The presence of copper and calcium divanadate in the diffractogram come essentially from heavy metals, as copper and vanadium, present in the phosphate sludge. Certainly, this phase would be formed after the thermal treatment.

Mineralogical and morphological characterization of light aggregates baked for 30 min.

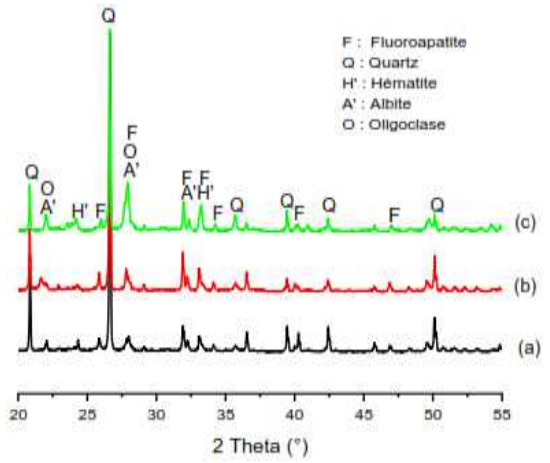

Figure 15. *X-ray diffractograms of S9 aggregates fired for 30 min at 900°C (a), 950°C (b) and 1000°C (c).*

X-ray diffractograms of S9 aggregates fired at 900°, 950° and 1000°C during 30 min are shown in Figure 15. The study of these diffractograms shows that they are mainly composed of fluoroapatite and quartz. From the initial composition of the mixture, we can deduce the disappearance of kaolinite in the aggregates. The reasons given for its disappearance in the light aggregates fired for 60 min are the same as for the aggregates fired for 30 min. As for the samples baked for 60 min the fluoroapatite detected are not carbonated. Moreover, we observed the insertion of the metalloid antimony in the structure of fluoroapatite to give $Ca_{5,17}Sb_{0,14}(PO_{4,138})_3F_{1,04}$. On the other hand, secondary phases have been detected in the diffractograms. They are albite, oligoclase and hematite. The albite and oligoclase phases belong to the plagioclase family as previously mentioned. The presence of these phases in the diffractograms is in agreement with the chemical composition of the mixed materials. Indeed, phosphate slurries, screenings and clay contain CaO, SiO_2 and Al_2O_3 which enter in the formation of plagioclases after a thermal transformation. It should also be remembered that oligoclase is an intermediate compound of the albite-anorthite series for an Ab/An ratio of 90/10 or 70/30.

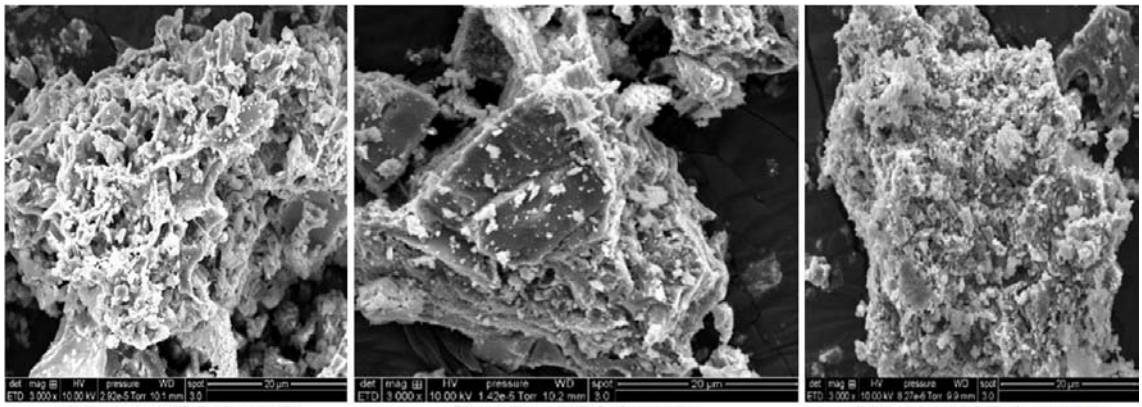

Figure 16. *SEM images of S9 aggregates sintered at 900°C, 950°C and 1000°C for 30 min at 3000x magnification.*

SEM analysis images of S9 aggregates fired at 900°, 950° and 1000°C for 30 min are shown in Figure 16. We observe on this figure that an abundant melt mass was formed which has as a consequence to alter and reduce the pores of the aggregates as the temperature increases.

X-ray diffractograms of S10 aggregates fired for 30 min at temperatures of 900°C, 950°C and 1000°C are shown in Figure 17. Their analyses show that they are also composed mainly of fluoroapatite and quartz. As for the S9 aggregates, we also observe secondary phases of oligoclase, albite and hematite. This appearance of secondary phases is related to the chemical composition of the raw materials mixed as expected in the S9 aggregates. We also notice the disappearance of kaolinite in agreement with the thermal analysis of the raw materials.

Quartz is still present in these aggregates but with quantities that decrease as the firing temperature increases. SEM image analyses (Figure 18a-c) show a very abundant melt, especially at 1000°C (Figure 18c). The abundance of the glass phase seems to be related to the partial melting of the fluoroapatite, considered as a self-melting agent. Under the effect of the increase of the quantity of this glass phase the porosity of the aggregates is reduced according to the temperature and their shape is more and more altered.

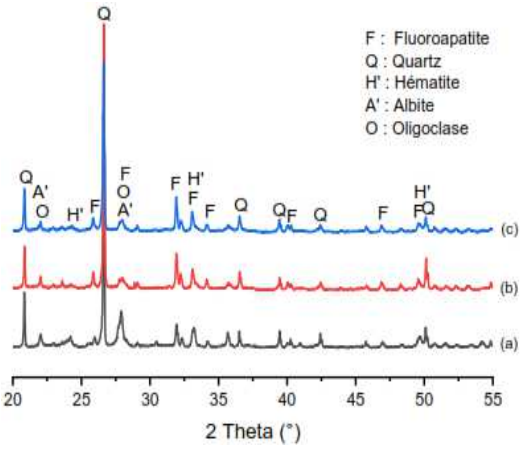

Figure 17. *X-ray diffractograms of S10 aggregates fired for 30 min at 900°C (a), 950°C (b) and 1000 °C (c).*

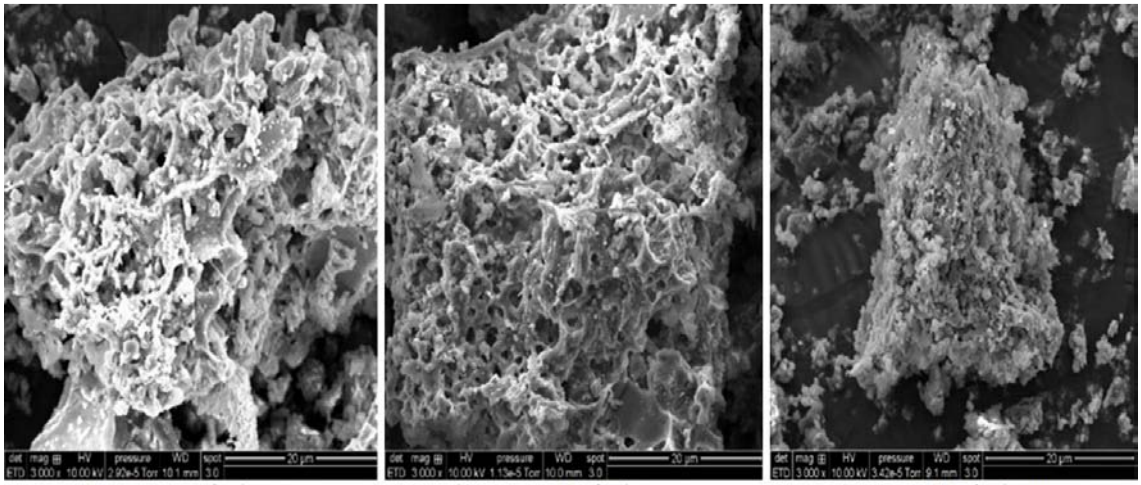

Figure 18. *SEM images of S10 aggregates fired for 30 min at 3000x magnification.*

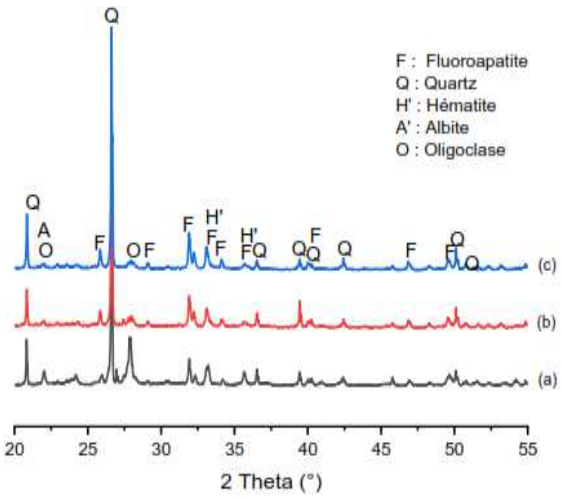

Figure 19. *X-ray diffractograms of S11 aggregates fired for 30 min at 900 °C (a), 950 °C (b) and 1000 °C (c).*

X-ray diffractograms of the S11 aggregates fired at temperatures of 900, 950 and 1000°C are shown in Figures 19a-c, while SEM images of the aggregates of the same samples are shown in Figures 20 a-c.

These diffractograms also reveal the presence of fluoroapatite and quartz phases as well as albite, oligoclase and hematite as secondary phases. We observe again, as for the aggregates S9 and S10, the transformation of quartz into amorphous silica which justifies the decrease in its quantity as the temperature increases [40]. As shown in the SEM images of Figure 20, the aggregates fired at high temperature were the site of glass phase formation. As in the case of S10 aggregates, here too, the increase in the amount of melted mass (glass phase), reduces the porosity with an alteration of the pore shape. Furthermore we observe rounded pseudo pores that are the result of the coalescence of the initial porosity, while the pores of polygonal geometry (Figure 20 b and c), would correspond to sites of detached fluoroapatite grains.

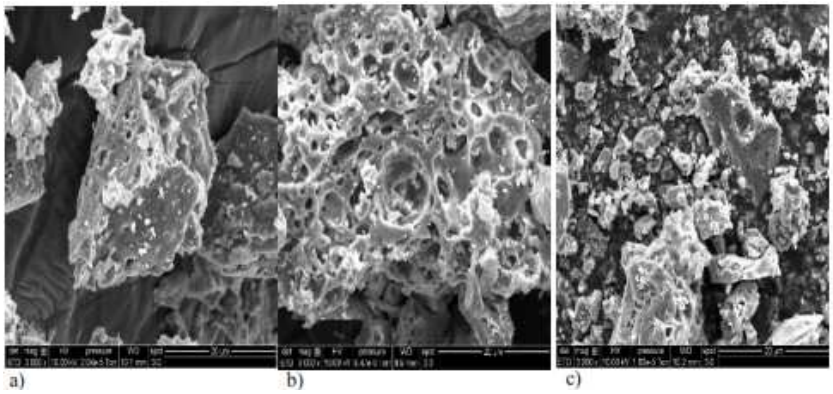

Figure 20. *SEM images of S11 aggregates baked at 900°C (a), 950°C (b) and 1000°C (c) for 30 min at 3000x magnification.*

4. Conclusion

The objective of this study is to examine the feasibility of manufacturing light aggregates from phosphate waste. The study of the chemical composition of these wastes revealed that this objective can only be achieved with phosphate sludge and screen rejects on the condition that they are enriched in aluminosilicate.

The enrichment of phosphate wastes in aluminosilicate

was carried out starting from the Aklakou clay whose characterization showed that it is mainly composed of silica and alumina, a good source of aluminosilicate amendment.

From the phosphate sludge and the screenings refusals, we elaborated three types of aggregates denoted S9, S10 and S11. The aggregates S9 and S10 have a homogeneous red-brown color on their whole surface. Cracks on the surface of these pellets are rarely visible. On the other hand, S11 aggregates have mostly pores and cracks reaching the surface of the pellets. Their color is grey to grey-black.

Water absorption of the aggregates fired for 30 min varies between 12.71% and 14.93% while that of the aggregates fired for 60 min varies between 12.78% and 15.16%. The lowest water uptake is observed in the S10 aggregates sintered at 900°C for 30 min while the highest water uptake is observed in the S9 aggregates sintered at 900°C for 60 min.

Dry density of the aggregates fired for 30 min varies between 1.27 and 1.68 g/cm^3 while that of the aggregates fired for 60 min varies between 1.75 and 2.13 g/cm^3. With the exception of the S11 aggregates fired at 950 and 1000°C for 60 min, which have their density above 2 g/cm^3, the others can be considered light. It should also be noted that the aggregates fired for 30 min have a lower density than the aggregates fired for 60 min.

Porosity of the aggregates baked for 30 min varies between 16.30 and 20%, while that of the aggregates baked for 60 min varies between 19.06 and 23.64%.

X-ray diffraction analysis of the aggregates shows that they are mainly composed of fluoroapatite and quartz. Apart from these phases, other secondary phases are also noted, such as hydroxyapatite, albite, labradorite, anorthite, hematite and copper and calcium divanadate. The study also showed that the amount of quartz and fluoroapatite decreases with temperature.

Based on the physical and mineralogical analyses carried out on the light aggregates, we could find for them agricultural applications, such as their use as substrates in hydroponics, in greenhouse cultivation in general, and in gardening. On the other hand, before using them in construction, in perspective, we must first determine their resistance to compression, which is an indispensable data.

Conflicts of Interest

The authors declare no conflicts of interest regarding the publication of this paper.

Acknowledgements

Authors would like to thank all the technical staff of different Laboratories in France (LAGEPP) and Canada (INRS) for their help for his acceptance to perform physicochemical characterization of our materials. This work was financially supported by the International Development Research Centre (IDRC) of Canada through the project FGéPro (Training in Industrial Process Engineering for Treatment and Valorization of Agricultural/Agroindustrial Waste in High Added Value Products).

References

[1] Roudié, P.: Une richesse nationale africaine. Les phosphates du Togo. Cahiers d'outre-mer. 30, 313–318 (1977). https://doi.org/10.3406/caoum.1977.2830.

[2] Agbossoumonde, D. Y.: Les problèmes liés à l'extraction des ressources naturelles au Togo : Le cas des phosphates de hahotoé-kpogamé et des calcaires de Tabligbo au Sud Togo. 10 (2011).

[3] Gnandi, K., Tobschall, H. J.: Heavy metal release from phosphorite tailings into seawater: a simulated laboratory study. Science of The Total Environment. 236, 181–190 (1999). https://doi.org/10.1016/S0048-9697(99)00279-X.

[4] Aduayi-Akue, A. A., Gnandi, K., Tete-Benissan, A., Degbe, M., Tanouayi, G., Gbeassor, M.: Evaluation des teneurs des métaux lourds dans le sang des sujets de la zone de traitement des phosphates au Sud du Togo. International Journal of Biological and Chemical Sciences. 9, 1972 (2015). https://doi.org/10.4314/ijbcs.v9i4.22.

[5] Gnandi, K., Tchangbedji, G., Killi, K., Baba, G., Abbe, K.: The Impact of Phosphate Mine Tailings on the Bioaccumulation of Heavy Metals in Marine Fish and Crustaceans from the Coastal Zone of Togo. Mine Water and the Environment. 25, 56–62 (2006). https://doi.org/10.1007/s10230-006-0108-4.

[6] Gnandi, K., Tobschall, H. J.: The pollution of marine sediments by trace elements in the coastal region of Togo caused by dumping of cadmium-rich phosphorite tailing into the sea. Environmental Geology. 38, 13–24 (1999). https://doi.org/10.1007/s002540050396

[7] Laursen, K., White, T. J., Cresswell, D. J. F., Wainwright, P. J., Barton, J. R.: Recycling of an industrial sludge and marine clay as light-weight aggregates. Journal of Environmental Management. 80, 208–213 (2006). https://doi.org/10.1016/j.jenvman.2005.08.026.

[8] Shathika Sulthana Begum, B., Gandhimathi, R., Ramesh, S. T., Nidheesh, P. V.: Utilization of textile effluent wastewater treatment plant sludge as brick material. Journal of Material Cycles and Waste Management. 15, 564–570 (2013). https://doi.org/10.1007/s10163-013-0139-4.

[9] Huang, C. H., Wang, S. Y.: Application of water treatment sludge in the manufacturing of lightweight aggregate. Construction and Building Materials. 43, 174–183 (2013). https://doi.org/10.1016/j.conbuildmat.2013.02.016.

[10] Anh Tuan, B. L., Tesfamariam, M. G., Chen, Y. Y., Hwang, C.-L., Lin, K. L., Young, M. P.: Production of Lightweight Aggregate from Sewage Sludge and Reservoir Sediment for High-Flowing Concrete. Journal of Construction Engineering and Management. 140, 04014005 (2014). https://doi.org/10.1061/(ASCE)CO.1943-7862.0000835.

[11] Boudaghpour, S., Hashemi, S.: A Study on Light Expended Clay Aggregate (LECA) in a Geotechnical View and its Application on Greenhouse and Greenroof Cultivation. INTERNATIONAL JOURNAL OF GEOLOGY. 2, 5 (2008).

[12] Chang, F. C., Lo, S.-L., Lee, M. Y., Ko, C.-H., Lin, J.-D., Huang, S. C., Wang, C.-F.: Leachability of metals from sludge-based artificial lightweight aggregate. Journal of Hazardous Materials. 146, 98–105 (2007). https://doi.org/10.1016/j.jhazmat.2006.11.069.

[13] Liu, D., Løkke, M. M., Leegaard Riis, A., Mortensen, K., Feilberg, A.: Evaluation of clay aggregate biotrickling filters for treatment of gaseous emissions from intensive pig production. Journal of Environmental Management. 136, 1–8 (2014). https://doi.org/10.1016/j.jenvman.2014.01.023.

[14] Corrochano, B. G., Azcárate, J. A., Gonzalez, M. R.: Heavy metal chemical fractionation and immobilization in lightweight aggregates produced from mining and industrial waste. International Journal of Environmental Science & Technology. 8, 667–676 (2011). https://doi.org/10.1007/BF03326251.

[15] Analysis of physical and mechanical properties of lightweight aggregate modified with sewage sludge. Proceedings of ECOpole. (2015). https://doi.org/10.2429/proc.2015.9(1)004.

[16] Fragoulis, D., Stamatakis, M. G., Chaniotakis, E., Columbus, G.: Characterization of lightweight aggregates produced with clayey diatomite rocks originating from Greece. Materials Characterization. 53, 307–316 (2004). https://doi.org/10.1016/j.matchar.2004.05.004.

[17] González-Corrochano, B., Alonso-Azcárate, J., Rodas, M.: Characterization of lightweight aggregates manufactured from washing aggregate sludge and fly ash. Resources, Conservation and Recycling. 53, 571–581 (2009). https://doi.org/10.1016/j.resconrec.2009.04.008.

[18] Anagnostopoulos, I. M., Stivanakis, V. E.: Utilization of lignite power generation residues for the production of lightweight aggregates. Journal of Hazardous Materials. 163, 329–336 (2009). https://doi.org/10.1016/j.jhazmat.2008.06.125.

[19] Mahmad Nor, A., Yahya, Z., Abdullah, M. M. A. B., Abdul Razak, R., Jaya Ekaputri, J., Faris, M. A., Nur Hamzah, H.: A Review on the Manufacturing of Lightweight Aggregates Using Industrial By-Product. MATEC Web of Conferences. 78, 01067 (2016). https://doi.org/10.1051/matecconf/20167801067.

[20] Ayati, B., Ferrándiz-Mas, V., Newport, D., Cheeseman, C.: Use of clay in the manufacture of lightweight aggregate. Construction and Building Materials. 162, 124–131 (2018). https://doi.org/10.1016/j.conbuildmat.2017.12.018.

[21] Loutou, M., Hajjaji, M., Mansori, M., Favotto, C., Hakkou, R.: Heated blends of clay and phosphate sludge: Microstructure and physical properties. Journal of Asian Ceramic Societies. 4, 11–18 (2016). https://doi.org/10.1016/j.jascer.2015.10.003.

[22] Olesik, J. W.: Elemental analysis using ICP-OES and ICP/MS. Analytical Chemistry. 63, 12A-21A (1991). https://doi.org/10.1021/ac00001a001.

[23] Ramsey, M. H., Potts, P. J., Webb, P. C., Watkins, P., Watson, J. S., Coles, B. J.: An objective assessment of analytical method precision: comparison of ICP-AES and XRF for the analysis of silicate rocks. Chemical Geology. 124, 1–19 (1995). https://doi.org/10.1016/0009-2541(95)00020-M.

[24] Ropp, R. C., Aia, M. A.: Thermal Analysis of Phosphor Raw Materials. Analytical Chemistry. 34, 1288–1291 (1962). https://doi.org/10.1021/ac60190a026.

[25] Schulze, D. G.: Differential X-Ray Diffraction Analysis of Soil Minerals. In: Amonette, J. E. and Stucki, J. W. (eds.) Quantitative Methods in Soil Mineralogy. pp. 412–429. Soil Science Society of America, Madison, WI, USA (2015).

[26] Whittig, L. D.: X-Ray Diffraction Techniques for Mineral Identification and Mineralogical Composition. In: Black, C. A. (ed.) Agronomy Monographs. pp. 671–698. American Society of Agronomy, Soil Science Society of America, Madison, WI, USA (2015).

[27] Koenig, J. L.: Application of Fourier Transform Infrared Spectroscopy to Chemical Systems. Applied Spectroscopy. 29, 293–308 (1975). https://doi.org/10.1366/000370275774455888.

[28] Kong, J., Yu, S.: Fourier Transform Infrared Spectroscopic Analysis of Protein Secondary Structures. Acta Biochimica et Biophysica Sinica. 39, 549–559 (2007). https://doi.org/10.1111/j.1745-7270.2007.00320.x.

[29] González-Corrochano, B., Alonso-Azcárate, J., Rodas, M.: Effect of prefiring and firing dwell times on the properties of artificial lightweight aggregates. Construction and Building Materials. 53, 91–101 (2014). https://doi.org/10.1016/j.conbuildmat.2013.11.099.

[30] Dondi, M., Cappelletti, P., D'Amore, M., de Gennaro, R., Graziano, S. F., Langella, A., Raimondo, M., Zanelli, C.: Lightweight aggregates from waste materials: Reappraisal of expansion behavior and prediction schemes for bloating. Construction and Building Materials. 127, 394–409 (2016). https://doi.org/10.1016/j.conbuildmat.2016.09.111.

[31] Hung, M. F., Hwang, C. L.: Study of fine sediments for making lightweight aggregate. Waste Management & Research. 25, 449–456 (2007). https://doi.org/10.1177/0734242X07077615.

[32] Yue, M., Yue, Q. Y., Qi, Y. F.: Effect of Sintering Temperature on the Properties of Sludge Ceramics and Fly-Ash Ceramics. Advanced Materials Research. 150–151, 1068–1072 (2010). https://doi.org/10.4028/www.scientific.net/AMR.150-151.1068.

[33] Terzić, A., Pezo, L., Mitić, V., Radojević, Z.: Artificial fly ash based aggregates properties influence on lightweight concrete performances. Ceramics International. 41, 2714–2726 (2015). https://doi.org/10.1016/j.ceramint.2014.10.086.

[34] Hashimoto, I., Jackson, M. L.: Rapid Dissolution of Allophane and Kaolinte-Halloysite after Dehydration. In: Ingerson, E. (ed.) Clays and Clay Minerals. pp. 102–113. Pergamon (2013).

[35] de Souza Santos, H., Wagner Campos, T., de Souza Santos, P., Kiyohara, P. K.: Thermal phase sequences in gibbsite/kaolinite clay: electron microscopy studies. Ceramics International. 31, 1077–1084 (2005). https://doi.org/10.1016/j.ceramint.2004.10.018.

[36] Khalfaoui, A., Hajjaji, M.: A Chloritic-illitic clay from Morocco: Temperature–time–transformation and neoformation. Applied Clay Science. 45, 83–89 (2009). https://doi.org/10.1016/j.clay.2009.03.006.

[37] Hajjaji, M., Khalfaoui, A.: Oil shale amended raw clay: Firing transformations and ceramic properties. Construction and Building Materials. 23, 959–966 (2009). https://doi.org/10.1016/j.conbuildmat.2008.05.017.

[38] Tchangbeddji, G., Djeteli, G., Ani Kili, K., Michel Savariault, J., Louis Lacout, J.: Chemical and structural characterization of natural phosphate of Hahotoe (Togo). Bull. Chem. Soc. Eth. 17, (2004). https://doi.org/10.4314/bcse.v17i2.61659.

[39] Konan K. L., Soro J., Andji J. Y. Y., Oyetola S., Kra G., "Etude comparative de la déshydroxylation/amorphisation dans deux kaolins de cristallinité différente" J. Soc. Ouest-Afr. Chim., 030. 29-39. August 2010.

[40] Loutou, M., Hajjaji, M., Mansori, M., Favotto, C., Hakkou, R.: Heated blends of phosphate waste: Microstructure characterization, effects of processing factors and use as a phosphorus source for alfalfa growth. Journal of Environmental Management, 177 (2016) 169–176. https://doi.org/10.1016/j.jenvman.2016.04.030.

[41] Koriko, M., Zounon, D., Tchegueni, S., Bafai, D. D., Degbe, K. A., Fiaty, K., Drogui, P. and Tchangbedji, G., Physicochemical and Mineralogical Characterizations of Wastes Coming from Phosphate Ore Processing of Hahotoe and Kpogame Mines. Journal of Minerals and Materials Characterization and Engineering, 9 (2021) 390-405. https://doi.org/10.4236/jmmce.2021.94027

[42] Koriko, M., Zounon, D., Degbe, A., Tchegueni, S., Bafai, D. D., Fiaty, K., Tchangbedji, G. and Drogui P., Caracterisations physico-chimiques et mineralogiques de l'argile d'Aklakou utilisee dans la poterie en vue de son application dans la formulation des agregats legers, Int. J. Adv. Res. 9 (09) (2021) 706-712. http://dx.doi.org/10.21474/IJAR01/13471

[43] Amrani, M., El Haloui, Y., Hajikarimi, P., Kchikach, A., Hakkou, R., Taha, Y., Towards the Valorization of Phosphate Wastes in bituminous materials. Academic Journal of Civil Engineering, 38 (1) (2020) 9-12. https://doi.org/10.26168/ajce.38.1.3

[44] Loutou, M., Taha, Y., Benzaazoua, M., Daafi, Y., Hakkou, R., Valorization of clay by-product from moroccan phosphate mines for the production of fired bricks, Journal of Cleaner Production, 229 (2019) 169-179. https://doi.org/10.1016/j.jclepro.2019.05.003

[45] Idrissi H., Taha Y., Elghali A., El Khessaimi Y., Aboulayt A., Amalik J., Hakkou R., Benzaazoua M., Sustainable use of phosphate waste rocks: From characterization to potential applications, Materials Chemistry and Physics, 260 (2021) 124119, https://doi.org/10.1016/j.matchemphys.2020.124119.

[46] El Machi A., Mabroum S., Taha Y., Tagnit-Hamou A., Benzaazoua M., Hakkou R., Valorization of phosphate mine waste rocks as aggregates for concrete, Materials Today: Proceedings, 37 (3) (2021) 3840-3846, https://doi.org/10.1016/j.matpr.2020.08.404